Combined FTIR Matrix Isolation and Ab Initio Studies of Pyruvic Acid: Proof for Existence of the Second Conformer

Igor D. Reva,*,†,‡ Stepan G. Stepanian,‡ Ludwik Adamowicz,§ and Rui Fausto†

Department of Chemistry, University of Coimbra, P 3004-535 Coimbra, Portugal, Institute for Low-Temperature Physics & Engineering of the National Academy of Sciences of Ukraine, 47 Lenin Ave., 61164 Kharkov, Ukraine, and Department of Chemistry, University of Arizona, Tucson, Arizona 85721

Received: January 11, 2001

The molecular structure of pyruvic acid was investigated by matrix isolation FTIR spectroscopy, density functional theory (DFT), and ab initio calculations performed at the RHF, MP2, MP4(SDQ), and CCSD(T) levels of theory with the aug-cc-pVDZ basis set. In these calculations, the geometries of the three lowest energy conformers of pyruvic acid were fully optimized at the DFT/B3LYP/aug-cc-pVDZ and MP2/aug-cc-pVDZ levels. Additionally, the relative energies of the conformers were calculated at the MP4, CCSD, and CCSD(T) levels. Harmonic frequencies and IR intensities were then calculated for these three conformers and were used to account for the zero point vibrational energy corrections and to assist the assignment of the observed bands to the different forms. We found that two conformers are present in the Ar matrix, and both forms exhibit a planar framework with the carbonyl bonds in a trans arrangement but differ in the orientation of the hydroxyl hydrogen. By varying the temperature of the pyruvic acid vapor prior to matrix deposition we were able to separate the bands due to the two conformers and measure their enthalpy difference. The spectral signature of the second pyruvic acid conformer has been identified for the first time. Experimental enthalpy difference between the two most stable conformers was found to be 8.7(±15%) kJ mol^{-1}, which is in good agreement with the theoretical result.

Introduction

Pyruvic acid, $CH_3-CO-COOH$, plays a fundamental role in biological systems. This molecule is also interesting from the viewpoint of structural chemistry, since it can assume different conformers due to intramolecular rotation along the single C−C and C−O bonds. Pyruvic acid is a similar system to natural amino acids, which we have studied before,[1−3] and like amino acids, shows an appreciable trend to decompose. In the case of the amino acids, we have shown that the low-temperature matrix isolation technique combined with IR spectroscopy can be successfully used to study these unstable compounds experimentally.[1−3] In the present work we applied the same approach to pyruvic acid.

Previous ab initio molecular orbital calculations on monomeric pyruvic acid[4,5] predicted the existence of four conformers, all exhibiting a planar heavy-atom framework with two methyl hydrogens symmetrically situated with respect to the molecular plane (Figure 1). In this work we will follow the nomenclature used for the pyruvic acid conformers in ref 4, which named conformers according to the magnitude of the CCC−O and CCOH angles. The upper-case letter (*C*, cis*; T*, trans) will refer to the CCC−O angle; the lower-case letter (*c* or *t*) will refer the CCOH angle.

Conformer *Tc* was found to be the lowest energy structure.[4−8] *Ct* and *Tt* species were predicted to have higher energies than

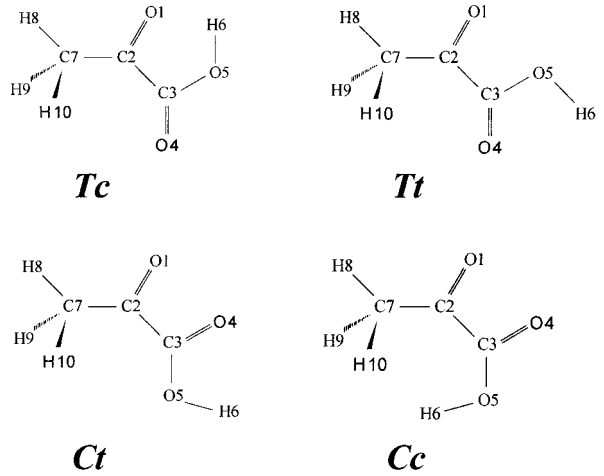

Figure 1. Conformers of pyruvic acid and atom numbering scheme.

Tc within the range 2−12 kJ mol^{-1}, depending on the level of calculation.[4] In relation to the experiment, this energy difference means that conformers *Tt* and *Ct*, along with *Tc*, could be present in the gas-phase pyruvic acid in noticeable amounts. The fourth possible conformer, *Cc*, has a much higher energy (from 44.93 to 52.80 kJ mol^{-1} above *Tc*[4]) and is of less experimental interest. Theoretical studies[6−8] analyzed in more detail the exact equilibrium arrangement of the methyl group in pyruvic acid. As found for other molecules bearing a methyl group adjacent to a carbonyl (e.g., acetic and thioacetic acids, acetone, acetaldehyde[9−11]), it is now well established that in pyruvic acid the methyl group assumes a conformation where one of the hydrogen atoms is syn periplanar with respect to the carbonyl

* Corresponding author. Tel.: +351 239 852 080. Fax: +351 239 827 703. E-mail: reva@qui.uc.pt.
† University of Coimbra.
‡ National Academy of Sciences of Ukraine.
§ University of Arizona.

10.1021/jp0101458 CCC: $20.00
Published on Web 04/20/2001

oxygen. The highest stability of this conformation is due to more favorable $\pi(CH_3) \rightarrow \pi^*(C{=}O)$ group orbital interactions and hyperconjugation through the σ bond system.[8,9]

Several microwave studies of gaseous pyruvic acid have been reported.[12−15] In consonance with the theoretical predictions, the main conclusion from these studies is that the most stable conformation is *Tc*. No other conformers have been experimentally found by this method. On the other hand, infrared studies of gaseous pyruvic acid[16] revealed the existence of two pyruvic acid forms at temperatures between 363 and 453 K. The most stable *Tc* conformer could be easily identified spectroscopically due to the observation of the low-frequency OH and C=O stretching bands associated with the intramolecularly hydrogen-bonded groups in this form. On the other hand, the precise nature of the second conformer could not be established, although it has been proposed that the conformation adopted by the hydroxyl group in this form is with all probability trans (i.e., the second observed conformer could be either *Tt* or *Ct*). Hollenstein, Akerman, and Günthard undertook a matrix isolation infrared study of sixteen isotopic modifications of pyruvic acid.[17] In that study, an assignment was proposed for the vibrational spectra of all isotopic species, assuming that only the *Tc* conformer contributes to the observed spectroscopic features. However, the possibility of the presence of a small amount of another pyruvic acid conformer was not excluded. The authors also mention the presence of detectable amounts of impurities in all the samples, such as water, carbon dioxide, and acetic acid. To the best of our knowledge, no other experimental infrared studies on pyruvic acid have been reported since the work of Hollenstein.

Since there were theoretical prerequisites (low predicted energy gap between conformers[4]) and experimental evidence (infrared detection of two conformers in the gaseous phase[16]) that pointed to the possibility of successfully using matrix isolation infrared spectroscopy to identify the precise nature of the low-energy conformers of pyruvic acid accessible to experiment, we decided to submit this compound to a new detailed study using this technique. High-level theoretical methods were used to assist the interpretation of the experimental data.

Experimental Section

Commercially available pyruvic acid (Aldrich, 98%) was used. Before the cryostat was cooled, a freeze−pump−thaw procedure was applied multiple times to the compound to remove volatile impurities. A glass vacuum system and standard manometric procedures were applied to deposit matrix gas (argon, Air Liquid, 99.9999%), which was used without further purification. The argon deposition rate during sample preparation was ca. 10 mmol/h.

Spectra were recorded on a Mattson FTIR spectrometer (Infinity 60AR series) in the range 4000−400 cm^{-1} with resolution 0.5 cm^{-1}. A DTGS mid-IR detector and a KBr beam splitter were used. A single-beam reference spectrum of the cold substrate was recorded before deposition of the matrix and was used by the spectrometer software as the background to calculate subsequent absorption spectra. All experiments have been done on the basis of the APD Cryogenics closed-cycle helium refrigeration system with a DE-202A expander. Necessary modifications of the sample compartment of the spectrometer were done in order to accommodate the cryostat head and allow purging of the instrument by a stream of dry air to remove water vapors. A KBr window was used as the optical substrate for matrices.

Pyruvic acid is known to readily undergo photodecomposition and its mechanism is found to be the unimolecular decarboxylation.[18−23] In view of the limited stability of the compound, we paid special attention to experimental conditions. For preparation of the matrices of pyruvic acid we employed a technique similar to that previously used to prepare samples of matrix-isolated formic acid.[24] The main idea consists of depositing pyruvic acid from a Knudsen cell protected against light. Such a cell, with shut-off possibility, has been built on the basis of an SS-4 BMRG micrometer valve (NUPRO). The sample compartment had a volume of about 1 mL and was glass-made, and precautions were taken in order to prevent exposure of the compound to light. The cell had two thermostatable parts: the valve nozzle and the sample compartment. Cooling of the sample compartment to 273 K was used to lower the saturated gas pressure over the liquid and achieving a better metering function of the valve. The exact sample-to-matrix ratios could not be measured in this layout. However, concentrations could be estimated indirectly by comparison to the spectra obtained for samples prepared using the standard manometric technique. This comparison enabled us to conclude that the samples deposited from the Knudsen cell were dilute enough to neglect association in the matrix. Annealing of the matrix up to 30 K revealed bands due to aggregates. These bands appear in the following regions: 1787−1773, 1745−1733, 1379−1373, 1363−1361, 1351−1337, 1225−1217, 1160−1151, 1128−1123, 975−970, 709−701, 683−675, and 669−667 cm^{-1}.

Theoretical Methods

In the present study both DFT and correlated level ab initio methods were used to estimate the relative conformational stabilities and the harmonic vibrational frequencies. The DFT calculations were performed with the B3LYP three-parameter density functional, which includes Becke's gradient exchange correction,[25] the Lee, Yang, Parr correlation functional,[26] and the Vosko, Wilk, Nusair correlation functional.[27] The standard Dunning's correlation-consistent double-ζ basis set augmented with s and p diffuse functions on hydrogen and s, p, and d diffuse functions on heavy atoms (the aug-cc-pVDZ basis set)[28−30] was used in the calculations.

The geometries of all pyruvic acid conformers were first fully optimized at the B3LYP/aug-cc-pVDZ and MP2/aug-cc-pVDZ levels of theory. This was followed by harmonic frequency calculations at these levels. The calculated frequencies were used to assist the analysis of the experimental spectra and to account for the zero-point vibrational energy contribution. The calculated harmonic frequencies were scaled down with two scaling factors: 0.96 for the O−H and C−H stretching vibrations and 0.99 for all other vibrations. In our previous studies on the conformational behavior of the nonionized amino acids[1,2] these scaling factors yielded the best agreement between the frequencies calculated with the aug-cc-pVDZ basis set and the observed ones. The relative stabilities of the pyruvic acid conformers were also calculated at the MP4, CCSD, and CCSD(T)/aug-cc-pVDZ levels of theory for the geometries optimized at the MP2/aug-cc-pVDZ level.

All calculations in this work were performed on IBM RS6000 workstations using Gaussian 98.[31]

Results and Discussion

Table 1 presents the optimized geometries of the three lowest energy conformational states of pyruvic acid calculated at the B3LYP/aug-cc-pVDZ and MP2/aug-cc-pVDZ levels of theory, their predicted rotational constants, and dipole moments. Previ-

TABLE 1: Optimized Geometry Parameters (Ångstroms and Degrees), Observed and Theoretical Rotational Constants (*A*, *B*, *C*, MHz), and Dipole Moments (μ, Debye) of the Pyruvic Acid Conformers Obtained in the DFT/B3LYP/aug-cc-pVDZ and MP2/aug-cc-pVDZ Calculations

	Tc			*Tt*		*Ct*	
	DFT	MP2	exptl[a,b]	DFT	MP2	DFT	MP2
			Bond Lengths				
O1C2	1.218	1.233	1.231	1.210	1.225	1.208	1.224
C2C3	1.551	1.545	1.523	1.550	1.543	1.557	1.550
C3O4	1.206	1.218	1.215	1.211	1.223	1.203	1.214
C3O5	1.338	1.347	1.328	1.342	1.351	1.358	1.367
O5H6	0.978	0.980	0.983	0.972	0.975	0.972	0.975
C2C7	1.496	1.499	1.486	1.504	1.507	1.507	1.509
C7H8	1.094	1.096	1.074	1.094	1.097	1.094	1.097
C7H9	1.099	1.101	1.106	1.099	1.101	1.099	1.101
C7H10	1.099	1.101	1.106	1.099	1.101	1.099	1.101
			Bond Angles				
O1C2C3	117.4	117.8	117.0	120.2	120.4	117.7	117.9
C2C3O4	123.1	123.0	122.0	122.9	122.8	124.3	124.6
C2C3O5	112.8	113.0	114.5	112.6	112.4	111.7	111.0
C3O5H6	106.7	105.6	105.2	107.2	105.9	107.2	106.0
C3C2C7	117.4	117.0	118.6	115.0	114.8	118.1	117.8
C2C7H8	110.0	109.8	110.7	109.3	109.2	109.3	109.1
C2C7H9	109.6	109.2	109.0	110.0	109.7	110.1	109.8
C2C7H10	109.5	109.2	109.0	110.0	109.7	110.1	109.8
			Dihedral Angles				
O1C2C3O4	180.0	180.0		180.0	180.0	0.0	0.0
O1C2C3O5	0.0	0.0		0.0	0.0	180.0	180.0
C2C3O5H6	0.0	0.0		180.0	180.0	180.0	180.0
O4C3C2C7	0.0	0.0		0.0	0.0	180.0	180.0
O1C2C7H8	0.0	0.0		0.0	0.0	0.0	0.0
O1C2C7H9	120.0	121.9		121.7	121.6	121.4	121.4
O1C2C7H10	−120.0	−121.9		−121.7	−121.6	−121.4	−121.4
A	5508.6	5427.2	5535.58	5608.9	5517.3	5535.9	5449.9
B	3558.4	3558.1	3583.35	3448.7	3460.4	3453.7	3465.8
C	2191.0	2178.2	2204.83	2164.1	2155.2	2155.2	2146.9
μ	2.42	2.63	2.30	1.28	1.47	4.08	4.52

[a] Experimental geometry from ref 14; [b] Experimental rotational constants and dipole moment from ref 13.

TABLE 2: Energies (Atomic Units) of the Lowest Energy Conformer *Tc* and Relative Stabilities Including the Zero Point Vibrational Energy[a] (kJ mol^{-1}) of the Pyruvic Acid Conformers Calculated at the Different Levels of Theory[b]

method	*Tc*	*Tt*	*Ct*	*Cc*
HF/6-31G*	−340.530595	4.8	13.3	52.5
HF/6-31++G**	−340.551873	4.8	13.1	
MP2/6-31G*	−341.438373	7.0	11.9	48.9
MP2/6-31++G**	−341.495882	6.9	11.4	
MP2/aug-cc-pVDZ	−341.579275	9.9	15.7	
MP4(SDQ)/6-31++G**//MP2/6-31++G**	−341.522542	6.1	10.2	
MP4(SDTQ)/6-31++G**//MP2/6-31++G**	−341.562217	6.5	10.3	
MP4(SDQ)/aug-cc-pVDZ//MP2/aug-cc-pVDZ	−341.607053	8.9	14.5	
CCSD/aug-cc-pVDZ//MP2/aug-cc-pVDZ	−341.602929	8.8	15.2	
CCSD(T)/aug-cc-pVDZ//MP2/aug-cc-pVDZ	−341.643200	9.6	15.7	
DFT/B3LYP/aug-cc-pVDZ	−342.458822	10.7	17.4	

[a] Zero point vibrational energies were scaled by applying the scaling factors 0.96 for the OH and CH stretching vibrations and 0.99 for all other vibrations at the DFT and MP2 levels and 0.9 for all vibrations at the HF level. [b] All relative energies were calculated with respect to the conformer *Tc*.

ously reported[13,14] experimental data for the most stable *Tc* conformer are also included in this table for comparison. Four pyruvic acid conformers (Figure 1) were found in the preliminary HF/6-31G* and MP2/6-31G* calculations but the more accurate calculations with the basis sets augmented with diffuse functions failed to locate conformer *Cc* at either the HF or MP2 levels of theory. In all cases optimizations converged to the lowest energy conformer *Tc*. Thus, we concluded that only three conformers (*Tc*, *Tt*, and *Ct*) are the true minima on the pyruvic acid potential energy surface. The zero-point vibrational-energy-corrected absolute energies for *Tc* calculated at different levels of theory and relative energies for other conformers are shown in Table 2.

The detailed analysis of the geometries predicted for the different conformers of pyruvic acid was already made in previous theoretical studies[6,8] and will not be repeated here. It is, however, worth noting that despite the fact that the general trends are essentially the same as discussed previously,[6,8] the higher level MP2 calculations presented in this study show a slightly better agreement with the experiment.[13,14] In particular, this concerns the bond angles, which are usually more difficult to accurately calculate than the bond lengths. Furthermore, the MP2/aug-cc-pVDZ predicted values for the C═O bond lengths are in considerably better agreement with the experimental values than the previous estimations obtained using other levels of theory and basis sets. The good agreement shown between

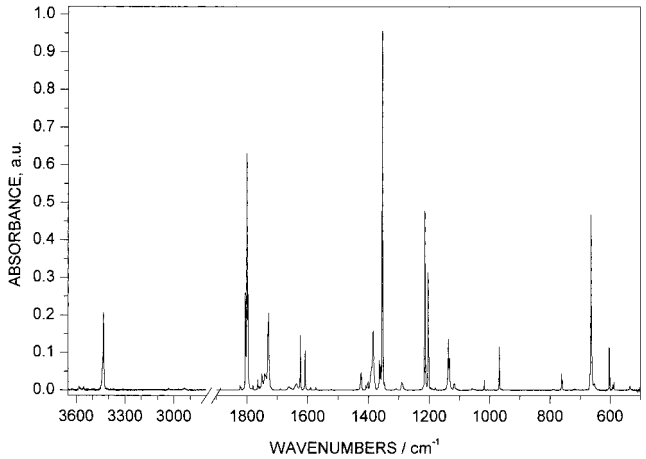

Figure 2. Infrared survey spectrum of pyruvic acid in an argon matrix (baseline subtracted. Deposition from a double thermostated Knudsen cell protected against light. Nozzle temperature, 296 K; optical substrate kept at 10 K during deposition).

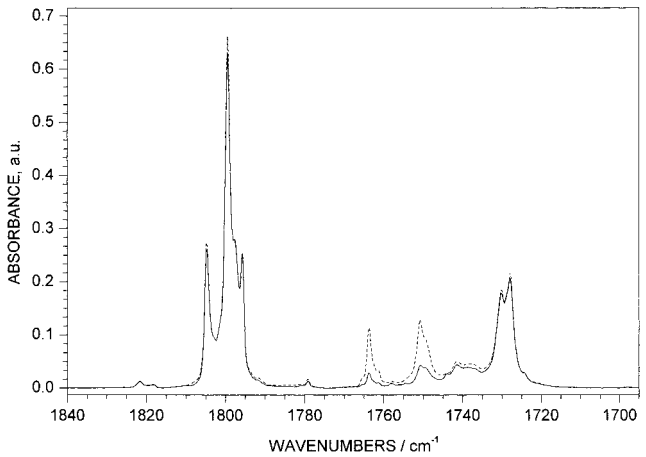

Figure 3. Infrared spectra (C═O stretching region) of pyruvic acid in argon matrices. Dashed line: deposition made at a nozzle temperature of 480 K; Solid line: deposition made at a nozzle temperature of 296 K. In both cases the compound compartment was kept at 273 K (ice−water bath) and the optical substrate kept at 10 K during the matrix deposition process. Baseline was subtracted from the spectra and then the spectra were normalized to the same intensity of the OH stretching vibration band of conformer *Tc* (see text).

the theoretical and experimental structural data gives us confidence in the general quality of the calculations of the vibrational properties.

All calculations yield conformer *Tt* more stable than conformer *Ct*. Except at the HF level, all calculations estimate an energy difference between *Ct* and *Tt* of ca. 4−6 kJ mol^{-1}. The energies of these two conformers in relation to the most stable form (*Tc*) are predicted by the ab initio methods within the ranges 4.8−9.9 and 10.2−15.7 kJ mol^{-1}, respectively, for *Tt* and *Ct* (see Table 2). The corresponding DFT/B3LYP/aug-cc-pVDZ-calculated values are 10.7 and 17.4 kJ mol^{-1}, and thus are similar to those obtained at the highest ab initio level of theory used, [CCSD(T)/aug-cc-pVDZ: 9.6 and 15.7 kJ mol^{-1}].

A typical survey infrared spectrum (fingerprint region) of pyruvic acid isolated in an argon matrix is shown in Figure 2. This spectrum strongly improves on the previously obtained data,[17] in particular concerning the absence of decomposition products, e.g., acetic acid (a detailed study of both thermal- and photodegradation of pyruvic acid, probed by matrix isolation infrared spectroscopy, has also been undertaken in our laboratory and will be the subject of a future publication). Minor bands

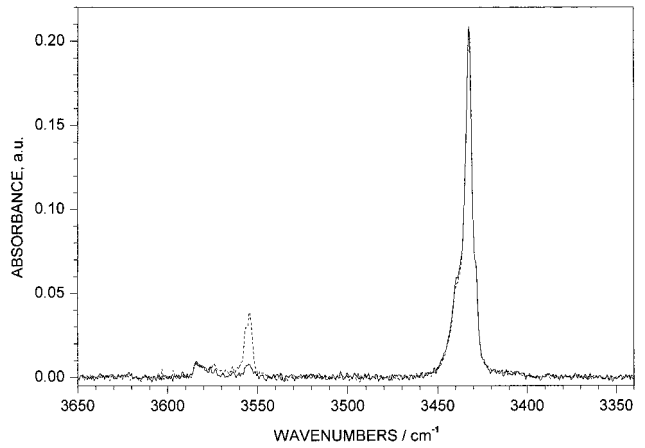

Figure 4. Infrared spectra (O−H stretching region) of pyruvic acid in argon matrices. See legend of Figure 3 for description of experimental conditions.

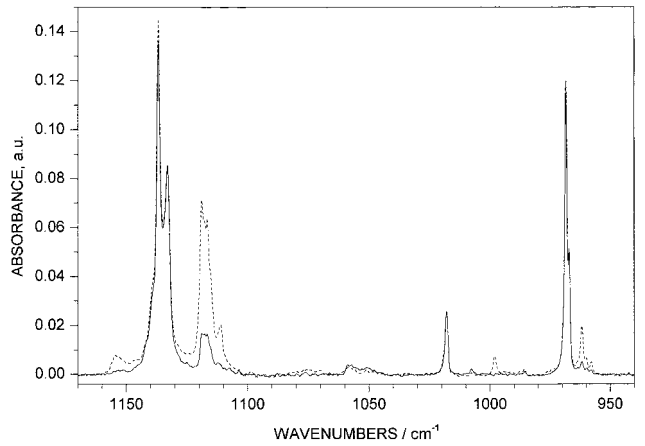

Figure 5. Infrared spectra (1170−940 cm^{-1} spectral region) of pyruvic acid in argon matrices. See legend of Figure 3 for description of experimental conditions.

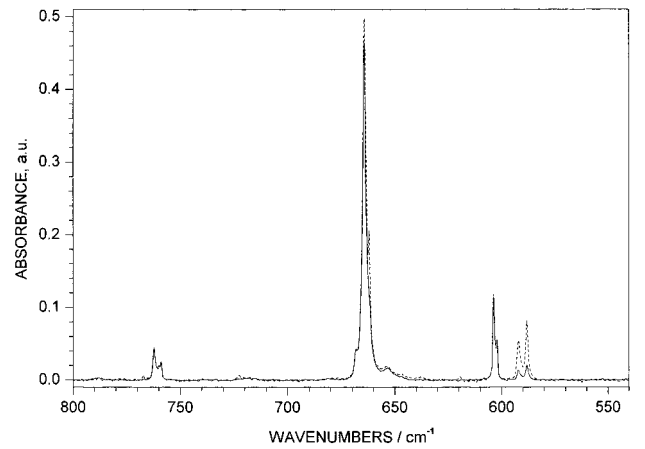

Figure 6. Infrared spectra (800−540 cm^{-1} spectral region) of pyruvic acid in argon matrices. See legend of Figure 3 for description of experimental conditions.

ascribable to traces of CO_2 and H_2O could still be observed in the spectrum, but these are unequivocally assigned to noninteracting well-isolated monomeric species.[32,33] Thus, we can firmly state that these substances do not interfere with the compound under study and its presence does not play any relevant role in the problems under analysis.

As mentioned in the *Introduction*, Hollenstein and collaborators had not excluded the possibility that some of the minor

TABLE 3: Observed (Ar Matrix, 10 K) and Calculated DFT/B3LYP/aug-cc-pVDZ and MP2/aug-cc-pVDZ Harmonic Frequencies (ν, cm^{-1}) and Intensities of the Pyruvic Acid Conformer *Tc*

obsd		calcd						
		DFT		MP2				
ν	I_{obs}[a]	ν	I_{calc}[b]	ν	I_{calc}[b]	ν	*c*, *g*	PED[d,g]
3584.2	0.009							2* (C3═O4 str)
3446.7	0.020							
3439.5	0.058							
3432.3	0.206	3467	111.9	3477	117.9	A′	ν(OH)	O5−H6 str [100]
3032.3	0.004	3041	4.9	3085	3.8	A′	ν(CH$_3$) as	C7−H8 str [78], C7−H9 str [11], C7−H10 str [11]
		2982	0.6	3037	0.4	A″	ν(CH$_3$) as	C7−H9 str [50], C7−H10 str [50]
2936.0	0.005	2924	0.5	2955	0.4	A′	ν(CH$_3$) s	C7−H9 str [38], C7−H10 str [38], C7−H8 str [22]
1821.6	0.010							δ(COH)+ δ(C2═O) Fermi resonance
1818.2	0.006							with ν(C3═O), see ref 17
1804.7	0.270							3* δ(C2═O) Fermi resonance with ν(C3═O), see ref 17
1799.5	0.646	1811	246.2	1791	193.2	A′	ν(C3═O)	C3═O4 str [84]
1797.6	0.268							
1795.7	0.248							
1791.7	0.022							
1730.2	0.183							
1727.9	0.212	1732	114.4	1715	65.3	A′	ν(C2═O)	C2═O1 str [86]
1423.7	0.051	1418	10.9	1439	10.2	A′	δ(CH$_3$) as	H10C7H9 bend [53], H8C7H9 bend [12], H8C7H10 bend [12], C2C7H8 bend [11]
1408.3	0.014	1413	13.2	1431	11.7	A″	δ(CH$_3$) as	H8C7H9 bend [37], H8C7H10 bend [37], C2C7H8 bend [20]
1406.1	0.010							
1403.4	0.017							
1401.2	0.025							
1389.5	0.065							
1384.5	0.162	1383	128.3	1397	92.8	A′	ν(C−C) as	C3O5H6 bend [21], C3−C2 str [15], C3−O5 str [13], C2−C7 str [11], C2C7H9 bend [11], C2C7H10 bend [11]
1364.1	0.087							
1359.3	0.067							
1354.6	0.946	1353	231.0	1357	221.8	A′	δ(CH$_3$) s	C2C7H9 bend [24], C2C7H10 bend [24], C3O5H6 bend [20], C2C7H8 bend [16]
1290.3	0.032							
1214.4	0.495	1232	86.8	1245	105.0	A′	δ(COH)	C3O5H6 bend [40], C3−C2 str [14],
1213.0	0.317							C2C7H8 bend [13], C2−C7 str [12]
1203.6	0.325							2* δ(C2═O) Fermi-resonance
1201.2	0.091							with δ(COH), see ref 17
1179.6	0.004							
1136.8	0.143	1139	58.1	1139	55.4	A′	ν(C−O)	C3−O5 str [46], C2C7H8 bend [14],
1133.0	0.086							C2−C7 str [12]
1017.8	0.027	1015	1.6	1015	1.0	A″	γ(CH$_3$)	C2C7H9 bend [27], C2C7H10 bend [27], O1C2C7H8 tor [21], O4C3C2C7 tor [18]
968.4	0.121	966	15.3	969	13.8	A′	γ(CH$_3$)	C2−C7 str [23], C2C7H8 bend [20],
967.1	0.05							C2C7H9 bend [12], C2C7H10 bend [12]
788	vw	757	8.8	762	12.0	A′	ν(C−C) s	C3−C2 str [33], C3−O5 str [17], C2−C7 str [16], C2C3O5 bend [12], C2C3O4 bend [11]
762.2	0.045	735	31.4	730	27.0	A″	γ(C3═O)	O1C2C3O5 tor [37], C2C3O5H6 tor [37]
758.9	0.025							
664.2	0.490	695	64.2	686	65.9	A″	τ(OH)	C2C3O5H6 tor [64], O4C3C2C7 tor [16]
653.2	0.021							
603.8	0.118	599	17.7	596	16.4	A′	δ(C2═O)	C3C2O1 bend [45], C2C3O5 bend [23], C2−C7 str [18]
602.2	0.042							
534.9	vw	519	3.3	521	3.0	A′	δ(C3═O)	C2C3O4 bend [52], C3−C2 str [16], C3C2C7 bend [16]
395.4[e]		394	16.6	386	15.7	A″	γ(C2═O)	O1C2C3O4 tor [81], O1C2C3O5 tor [12]
393.4[e]								
388.4[e]		383	10.2	384	9.4	A′	δ(CCO)	C2C3O5 bend [36], C3C2C7 bend [22], C3C2O1 bend [18], C3−C2 str [17]
258.0[e]		247	26.4	246	24.3	A′	δ(CCC)	C3C2C7 bend [47], C2C3O4 bend [20], C2C3O5 bend [20], C3C2O1 bend [11]
∼134[f]		127	0.3	135	0.1	A″	τ(CH$_3$)	O1C2C7H9 tor [34], O1C2C7H10 tor [34], O1C2C7H8 tor [27]
124[e]		91	8.1	94	7.0	A″	τ(C−C)	O1C2C3O5 tor [52], O4C3C2C7 tor [48]
115[e]								

[a] I_{obs} - Relative peak intensities (au), corresponding to deposition at nozzle temperature 480 K. [b] I_{calc} − calculated intensities in km mol^{-1}, values less than 0.05 rounded to zero. [c] Approximate description: ν − stretching, δ − bending, γ − rocking, τ − torsion. [d] Potential energy distributions (PED) calculated at MP2 level are given in square brackets. Only contributions of 10% are listed. [e] Low-frequency modes (below 400 cm^{-1}) not studied experimentally in the present work. Experimental values and assignments were taken from ref 17. [f] Microwave estimate from ref 14. [g] Abbreviations: str, stretching; bend, bending; tor, torsion; sh, shoulder; vw, very weak; as, asymmetrical; s, symmetrical.

bands they left unassigned in their study were due to a conformer other than the most stable *Tc* form.[17] To test this hypothesis, we recorded new spectra of matrix-isolated pyruvic acid using different Knudsen cell nozzle temperatures. Expansions of some selected spectral regions showing the spectra obtained at 296 and 480 K are presented in Figures 3−6. The spectra were

TABLE 4: Observed (Ar Matrix, 10 K) and Calculated DFT/B3LYP/aug-cc-pVDZ and MP2/aug-cc-pVDZ Harmonic Frequencies (ν, cm^{-1}) and Intensities of the Pyruvic Acid Conformer *Tt*

obsd		calcd						
		DFT		MP2				
ν		ν	I_{calc}[b]	ν	I_{calc}[b]		c	PED[d]
3556.1	0.040	3588	77.1	3582	89.7	A′	ν(OH)	O5−H6 str [100]
3554.1	0.041							
		3040	5.5	3083	4.2	A′	ν(CH$_3$) as	C7−H8 str [77], C7−H9 str [11], C7−H10 str [11]
		2983	2.1	3037	1.6	A″	ν(CH$_3$) as	C7−H9 str [50], C7−H10 str [50]
		2923	0.0	2954	0.2	A′	ν(CH$_3$) s	C7−H9 str [39], C7−H10 str [39], C7−H8 str [22]
1763.7	0.126	1781	295.2	1756	209.4	A′	ν(C3═O)	C3═O4 str [86]
1761.4	0.039							
1750.8	0.138	1770	118.5	1730	102.8	A′	ν(C2═O)	C2═O1 str [88]
1749.4	sh							
		1420	10.1	1442	9.5	A′	δ(CH$_3$) as	H10C7H9 bend [56], H8C7H9 bend [12], H8C7H10 bend [12]
		1415	13.3	1432	12.0	A″	δ(CH$_3$) as	H8C7H9 bend [37], H8C7H10 bend [37], C2C7H8 bend [22]
		1375	0.2	1397	4.3	A′	ν(C−C) as	C3−O5 str [21], C3−C2 str [17], C3O5H6 bend [15], C2C3O4 bend [13]
		1347	47.5	1355	46.0	A′	δ(CH$_3$) s	C2C7H9 bend [28], C2C7H10 bend [28], C2C7H8 bend [17], C3O5H6 bend [10]
		1211	37.7	1221	26.3	A′	δ(COH)	C3O5H6 bend [46], C2−C7 str [13], C2C7H8 bend [11], C3C2O1 bend [10]
1118.8	0.077	1126	227.2	1124	236.4	A′	ν(C−O)	C3−O5 str [39], C2C7H8 bend [16], C3O5H6 bend [15], C2−C7 str [11]
1116.6	0.069							
1111.0	0.023							
		1015	1.3	1015	1.0	A″	γ(CH$_3$)	C2C7H9 bend [28], C2C7H10 bend [28], O1C2C7H8 tor [19], O4C3C2C7 tor [18]
961.9	0.023	957	35.8	963	33.9	A′	γ(CH$_3$)	C2−C7 str [25], C2C7H8 bend [19], C2C7H9 bend [12], C2C7H10 bend [12]
957.9	0.006							
		731	9.4	741	4.6	A′	ν(C−C) s	C3−C2 str [32], C3−O5 str [19], C2−C7 str [19], C2C3O5 bend [10]
722.7	vw	719	42.3	714	39.1	A″	γ(C3═O)	O1C2C3O5 tor [48], O4C3C2C7 tor [20], O1C2C3O4 tor [10]
716.4	vw							
588.2[e]	0.088	623	86.5	627	86.2	A″	τ(OH)	C2C3O5H6 tor [85]
592.1[e]	0.062	585	75.9	582	75.5	A′	δ(C2═O)	C3C2O1 bend [36], C2C3O5 bend [27], C2−C7 str [14], C2C3O4 bend [10]
		507	1.8	511	1.9	A′	δ(C3═O)	C2C3O4 bend [47], C3−C2 str [15], C3C2O1 bend [14], C3C2C7 bend [14]
		382	1.0	383	0.9	A′	δ(CCO)	C3C2C7 bend [32], C2C3O5 bend [30], C3−C2 str [20], C3C2O1 bend [16]
		379	0.1	375	0.2	A″	γ(C2═O)	O1C2C3O4 tor [81], O1C2C3O5 tor [12]
		244	10.1	243	9.1	A′	δ(CCC)	C3C2C7 bend [38], C2C3O5 bend [26], C2C3O4 bend [21], C3C2O1 bend [14]
		129	0.0	143	0.0	A″	τ(CH$_3$)	O1C2C7H9 tor [35], O1C2C7H10 tor [35], O1C2C7H8 tor [31]
		34	7.6	41	6.6	A″	τ(C−C)	O1C2C3O5 tor [59], O4C3C2C7 tor [56], O1C2C3O4 tor [13]

[a,b,c,d,g] See footnotes to Table 3. [e] Assignment based on the frequency order or intensity values is ambiguous. Tentative assignment is made on the basis of the frequency shifts relative to the analogous vibrations of conformer *Tc*.

normalized to the same intensity of the OH stretching vibration of conformer *Tc*, since ν(OH) mode in this conformer is predicted by the calculations to have a clearly distinct frequency when compared with the same mode in any other conformer. It is clear from these figures that several absorptions increase their intensities relative to the bands due to conformer *Tc* upon increasing the temperature of the nozzle. Taking into consideration the theoretical results (both structural and vibrational data) now obtained, we were able to unequivocally assign these bands to conformer *Tt*, as described in detail below.

Tables 3 and 4 summarize the assignments now made for the two experimentally observed conformers of pyruvic acid. These tables present the observed frequencies, intensities, and the corresponding calculated values obtained using the DFT and MP2 methods, together with the calculated potential energy distributions (PED). Table 5 shows the calculated data for conformer *Ct*.

All bands assigned to conformer *Tt* increase their intensity in a concerted way when increasing the temperature of the nozzle relative to those bands that originated in the conformational ground state, in consonance with the higher energy of the *Tt* form. In Figures 3-6, these bands can be easily noticed. We shall start by discussing in detail the results shown in Figure 3 (ν(C═O) stretching spectral region) since these are particularly relevant to prove the identity of the second observed conformer.

In the ν(C═O) stretching region the two vibrations of conformer *Tc* give rise to the doublet of bands at 1730.2 and 1727.9 cm^{-1} (ν(C2═O1)) and to the set of bands in the region 1791−1800 cm^{-1} (ν(C3═O4)). In both cases, the observed splitting can be attributed to matrix site effects, due to existence of different local environments around the matrix-isolated pyruvic acid molecules (it is well-known that this phenomenon is particularly noticeable for vibrations involving large transition dipole moments, as is the case of carbonyl stretching modes). The low-intensity doublet at 1821.6 and 1818.2 cm^{-1} and the more intense band at 1804.7 cm^{-1} are due to the δ(COH) + δ(C2═O1) combination and the 3*(δ(C2═O1)) overtone vibrations of *Tc* in Fermi resonance with ν(C3═O4), as previously demonstrated by Hollenstein and collaborators.[17] The two carbonyl stretching vibrations of the *Tt* conformer are observed as site-split doublets at 1763.7/1761.4 cm^{-1} (ν(C3═O4)) and 1750.8/1749.4 cm^{-1} (ν(C2═O1)). Noteworthy, in consonance with the assignment of these bands to conformer *Tt*, the difference between the average frequencies of the two doublets is ≈13 cm^{-1}, being of the same order of magnitude of the predicted values for the *Tt* conformer (MP2: 11 cm^{-1}, DFT: 26 cm^{-1}) and clearly distinct from the calculated values for the *Ct* form (MP2, 72 cm^{-1}; DFT, 57 cm^{-1}).

The small band observed at 1779.0 cm^{-1} is due to traces of acetic acid,[34] while the low-intensity features observed around 1787−1783 and 1745−1733 cm^{-1} are due to a minor percentage of aggregated pyruvic acid. We shall stress that these bands correspond to the most intense infrared absorptions of these species. Furthermore, in the case of acetic acid, the analogical band corresponds to the single feature that could be clearly observed in the spectrum. These results clearly prove that, as mentioned in the Experimental Section, both degradation of the

TABLE 5: Calculated DFT/B3LYP/aug-cc-pVDZ and MP2/aug-cc-pVDZ Harmonic Frequencies (ν, cm^{-1}) and Intensities (I, km mol^{-1}) of the Pyruvic Acid Conformer *Ct*

DFT		MP2				
ν	I^a	ν	I^a		c	PED[b,c]
3579	67.3	3576	83.5	A′	ν(OH)	O5−H6 str [100]
3034	7.2	3078	5.3	A′	ν(CH$_3$) as	C7−H8 str [71], C7−H9 str [12], C7−H10 str [12]
2982	2.7	3036	2.0	A″	ν(CH$_3$) as	C7−H9 str [47], C7−H10 str [47]
2921	0.1	2952	0.3	A′	ν(CH$_3$) s	C7−H9 str [37], C7−H10 str [37], C7−H8 str [19]
1808	150.3	1788	167.7	A′	ν(C3═O)	C3═O4 str [85]
1736	227.9	1731	110.6	A′	ν(C2═O)	C2═O1 str [86]
1425	10.3	1445	9.7	A′	δ(CH$_3$) as	H10C7H9 bend [49], H8C7H9 bend [13], H8C7H10 bend [13], C2C7H8 bend [12]
1418	24.6	1436	26.5	A″	δ(CH$_3$) as	H8C7H9 bend [35], H8C7H10 bend [35], C2C7H8 bend [19]
1357	46.0	1366	51.1	A′	δ(CH$_3$) s	C2C7H9 bend [31], C2C7H10 bend [31], C2C7H8 bend [20], C2−C7 str [11]
1323	10.7	1336	16.7	A′	δ(COH)	C3O5H6 bend [34], C3−O5 str [19], C3−C2 str [12], C2C3O4 bend [10]
1177	109.7	1192	84.5	A′	ν(C−C) as	C3O5H6 bend [33], C2−C7 str [20], C2C7H8 bend [19], C3−C2 str [10], C3C2O1 bend [10]
1119	218.5	1112	234.2	A′	ν(C−O)	C3−O5 str [48], C3O5H6 bend [16]
1019	1.5	1017	1.2	A″	γ(CH$_3$)	C2C7H10 bend [29], C2C7H9 bend [29], O1C2C3O4 tor [25], O1C2C7H8 tor [19]
964	19.2	971	13.8	A′	γ(CH$_3$)	C2C7H8 bend [23], C2−C7 str [22], C2C7H9 bend [14], C2C7H10 bend [14]
722	8.8	730	4.0	A′	ν(C−C) s	C3−C2 str [33], C3−O5 str [19], C2−C7 str [15], C2C3O4 bend [10]
721	49.3	714	45.8	A″	γ(C2═O)	O1C2C3O4 tor [74], O1C2C3O5 tor [11], C2C3O5H6 tor [10]
619	77.4	619	78.5	A″	τ(OH)	C2C3O5H6 tor [79], O1C2C3O4 tor [12]
601	38.4	600	35.8	A′	δ(C2═O)	C3C2O1 bend [37], C2C3O4 bend [30], C2−C7 str [18]
475	8.4	477	11.1	A′	δ(CCO)	C2C3O5 bend [59], C3C2C7 bend [18]
393	3.5	395	3.3	A′	δ(C3═O)	C3C2C7 bend [29], C2C3O4 bend [26], C3−C2 str [24], C3C2O1 bend [20]
384	0.0	377	0.0	A″	γ(C3═O)	O4C3C2C7 tor [50], O1C2C3O5 tor [36]
251	1.2	253	1.2	A′	δ(CCC)	C3C2C7 bend [38], C2C3O5 bend [29], C2C3O4 bend [19], C3C2O1 bend [13]
153	0.1	169	0.0	A″	τ(CH$_3$)	O1C2C7H9 tor [36], O1C2C7H10 tor [36], O1C2C7H8 tor [28]
22	0.3	27	0.3	A″	τ(C−C)	O1C2C3O5 tor [58], O4C3C2C7 tor [41]

[a] Values less than 0.05 rounded to zero. [b] Potential energy distributions (PED) calculated at MP2 level are given in square brackets. Only contributions ≥10% are listed. [c] Abbreviations and approximate description, see footnotes to Table 3.

sample and aggregation could be almost completely avoided in our experiments.

In the ν(O−H) stretching region (Figure 4), the bands originated in the two conformers could be easily observed. The most stable *Tc* conformer gives rise to the intense band (split due to matrix-site effects) near 3440 cm^{-1}, while conformer *Tt* originates the doublet near 3555 cm^{-1}. The observed red shift in the ν(OH) mode of conformer *Tc*, due to the presence in this form of the intramolecular hydrogen bond, is ca. 115 cm^{-1} (taking as the reference value the frequency of the *Tt* form). This indicates that the hydrogen bond in the most stable conformer of pyruvic acid is considerably stronger. For instance, it is stronger than in oxalic (HOOCCOOH) and glycolic (CH_2-OHCOOH) acids, where the corresponding values for $\Delta\nu$(OH) were found to be 70 and 80 cm^{-1}, respectively,[35,36] though it is considerably weaker than in neutral glycine (CH_2NH_2COOH; $\Delta\nu$(OH) = 360 cm^{-1})[1] and malonic acid ($HOOCCH_2COOH$; $\Delta\nu$(OH) = 295 cm^{-1}).[37] The feature at 3584.2 cm^{-1} we assign to the first overtone of the C3═O4 stretching vibration of conformer *Tc*.

Figure 5 shows the spectral region between 1170 and 940 cm^{-1}. This is the region where the bands due to the ν(C−O) stretching and methyl rocking modes (γ(CH$_3$) A″ and γ(CH$_3$) A′) are predicted (see Tables 3 and 4). The vibrations of the *Tc* conformer are easily ascribed to the most intense bands appearing in this region at 1136.8/1133.0, 1017.8, and 968.4/967.1 cm^{-1}, respectively, with the doublets due to site splitting effects. Conformer *Tt* gives rise to the bands that increase with the temperature of the nozzle; those are observed at 1118.8/1116.6/1111.0 cm^{-1} (ν(C−O)) and 961.9/957.9 cm^{-1} (γ(CH$_3$) A′). The very low intensity of the γ(CH$_3$) A″ mode in this conformer (see Table 4) prevents its experimental observation. Most of the remaining (low-intensity) bands observed in this spectral region could be identified as due to aggregates (1160−1151, 975−970 cm^{-1}), or combination tones (e.g., the doublet around 1050 cm^{-1} is ascribed to τ(OH) + γ(C2═O1), the combination mode of *Tc*). The origin of the small bands at 1007.7 and 998.2 cm^{-1} still requires further investigation, but there is some evidence suggesting that the low-frequency band is associated with thermal degradation in the gas phase prior to deposition.

In the 800−540 cm^{-1} spectral region (Figure 6), the δ(C2═O1), τ(OH), and γ(C3═O4) vibrations of the *Tc* conformer are assigned to the bands at 603.8/602.2, 664.2, and 762.2/758.9 cm^{-1}, respectively. In agreement with the relative position predicted by the calculations (see Tables 3 and 4), the corresponding bands due to the *Tt* conformer are observed at 592.1, 588.2, and 722.7/716.4 cm^{-1}. Besides these bands, the low-intensity band at ca. 788 cm^{-1} is now assigned to the ν(C3−C2) vibration of the *Tc* conformer. This band was not assigned by Hollenstein and collaborators.[17] The ν(C3−C2) mode ascribed by these authors to the doublet at 762.2/758.9 cm^{-1} is now reassigned to γ(C3═O4). In ref 17, γ(C3═O4) was assigned to the doublet at 722.7/716.4 cm^{-1} which, however, could now be assigned to the *Tt* conformer, since it follows the general pattern of variation of intensity with the nozzle temperature of all other bands assigned to this conformer. In the same spectral region, the band at 653.2 cm^{-1} is assigned to the γ(C2═O1) + δ(CCC) combination tone of the *Tc* conformer, whose fundamentals were observed at 395.4/393.4 and 258.0 cm^{-1}, respectively,[17] while the small shoulder at ca. 670 cm^{-1} is due to aggregates. Finally, the band at 662.0 cm^{-1}, which is clearly visible in the spectrum obtained using the highest nozzle temperature, is due to isolated CO_2, which appears in the matrix as a decomposition product. Dahoo et al. investigated the spectrum of CO_2 isolated in argon matrixes[32] and they were able to observe bands at 661.9 and 663.8 cm^{-1} due to the degenerated bending modes of CO_2 isolated in two different matrix sites. It is important to note that by subtracting the two spectra of pyruvic acid shown in Figure 6, obtained using different nozzle temperatures, the second band due to the bending modes of CO_2 becomes clearly visible. This band is

superimposed with the 664.2 cm^{-1} band of pyruvic acid and contributes somewhat (ca. 6%) to the total intensity of the observed spectral feature.

Assuming that, in a relatively narrow region $T_1 - T_2$, the change in entropy is negligible and that the shift of the conformational equilibrium $K = K_{ij}(T_2)/K_{ij}(T_1) = I_j(T_2)/I_j(T_1)$, the enthalpy difference ΔH_{ij} can be derived from the ratio of the integral intensity of conformer bands using eq 1, when the spectra are rescaled to equal intensities I_i of the bands of conformer i at T_2 and T_1.

$$\Delta H_{ij} = RT_1T_2/(T_2 - T_1) \ln[K_{ij}(T_2)/K_{ij}(T_1)] \qquad (1)$$

The integrated intensities corresponding to the bands assigned to ν(OH), ν(C2═O1), ν(C3═O4), ν(C−O), $\gamma(CH_3)$ A′ and the pair of bands τ(OH)/δ(C2═O1) (see Figures 3−6) were used for the calculation of ΔH_{ij}, yielding an average value of 8.7-(±15%) kJ mol^{-1}. This value is of the same order of magnitude of the previous estimation obtained for the gaseous phase using the ν(O−H) infrared intensities [9.8(±14%) kJ mol^{-1}],[16] and very close to our best calculated value for ΔE (9.6 kJ mol^{-1}; see Table 2).

Conclusion

This work reports a matrix isolation spectroscopic and theoretical ab initio and DFT study of pyruvic acid. Use of the double-thermostated Knudsen cell permitted us to identify for the first time the spectral signature of a second conformer of pyruvic acid. This was shown to be the *Tt* conformer, whose observed enthalpy difference relative to the most stable *Tc* conformer for the argon isolated compound is estimated to be 8.7(±15%) kJ mol^{-1}.

Acknowledgment. We acknowledge the financial support of the *NATO Science Fellowship* (grant ICCTI, #0643 09/08'99) and the *Fundação para a Ciência e a Tecnologia*, Lisbon (research project PRAXIS/QUI/10137/98 and grant FCT #SFRH/BPD/1661/2000). L.A.'s contribution to this project was supported by a grant from the National Science Foundation.

References and Notes

(1) Stepanian, S. G.; Reva, I. D.; Radchenko, E. D.; Rosado, M. T. S.; Duarte, M. L. T. S.; Fausto, R.; Adamowicz, L. *J. Phys. Chem. A* **1998**, *102*, 1041.
(2) Stepanian, S. G.; Reva, I. D.; Radchenko, E. D.; Adamowicz, L. *J. Phys. Chem. A* **1998**, *102*, 4623.
(3) Stepanian, S. G.; Reva, I. D.; Radchenko, E. D.; Adamowicz, L. *J. Phys. Chem. A* **1999**, *103*, 4404.
(4) Murto, J.; Raaska, T.; Kunttu, H.; Räsänen, M. *THEOCHEM* **1989**, *200*, 93.
(5) Chen, C.; Shyu, S.-F. *THEOCHEM* **2000**, *503*, 201.
(6) Van Alsenoy, C.; Schäfer, L.; Siam, K.; Ewbank, J. D. *THEOCHEM* **1989**, *187*, 271.
(7) Tarakeshwar, P.; Manogaran, S. *THEOCHEM* **1998**, *430*, 51.
(8) Zhou, Z. Y.; Du, D. M.; Fu, A. P. *Vibr. Spectrosc.* **2000**, *23*, 181.
(9) Fausto, R.; Batista de Carvalho, L. A. E.; Teixeira-Dias, J. J. C. *THEOCHEM* **1990**, *207*, 67.
(10) Liao, D. W.; Mebel, A. M.; Hayashi, M.; Shiu, Y. J.; Chen, Y. T.; Lin, S. H. *J. Chem. Phys.* **1999**, *111*, 205.
(11) Nösberger, P.; Bauder, A.; Günthard, Hs. H. *Chem. Phys.* **1973**, *1*, 418.
(12) Kaluza, C. E.; Bauder, A.; Günthard, Hs. H. *Chem. Phys. Lett.* **1973**, *22*, 454.
(13) Marstokk, K.-M.; Møllendal, H. *J. Mol. Struct.* **1974**, *20*, 257.
(14) Dyllick-Brenzinger, C. E.; Bauder, A.; Günthard, Hs. H. *Chem. Phys.* **1977**, *23*, 195.
(15) Meyer, R.; Bauder, A. *J. Mol. Spectrosc.* **1982**, *94*, 136.
(16) Schellenberger, A.; Beer, W.; Oehme, G. *Spectrochim. Acta* **1965**, *21*, 1345.
(17) Hollenstein, H.; Akermann, F.; Günthard, Hs. H. *Spectrochim. Acta A* **1978**, *34*, 1041.
(18) Buechele, J. L.; Weitz, E.; Lewis, F. D. *Chem. Phys. Lett.* **1981**, *77*, 280.
(19) Wood, C. F.; O'Neill, J. A.; Flynn, G. W. *Chem. Phys. Lett.* **1984**, *109*, 317.
(20) Rosenfeld, R. N.; Weiner, B. *J. Am. Chem. Soc.* **1983**, *105*, 3485.
(21) Yadav, J. S.; Goddard, J. D. *J. Chem. Phys.* **1986**, *85*, 3975.
(22) Räsänen, M.; Raaska, T.; Kunttu, H.; Murto, J. *THEOCHEM* **1990**, *208*, 79.
(23) Norris, K. E.; Bacskay, G. B.; Gready, J. E. *J. Comput. Chem.* **1993**, *14*, 699.
(24) Reva, I. D.; Plokhotnichenko, A. M.; Radchenko, E. D.; Sheina, G. G.; Blagoi, Yu. P. *Spectrochim. Acta A* **1994**, *50*, 1107.
(25) Becke, A. D. *Phys. Rev. B* **1988**, *38*, 3098.
(26) Lee, C.; Yang, W.; Parr, R. G. *Phys. Rev. B* **1988**, *37*, 785.
(27) Vosko, S. H.; Wilk, L.; Nusair, M. *Can. J. Phys.* **1980**, *58*, 1200.
(28) Woon, D. E.; Dunning, T. H. *J. Chem. Phys.* **1993**, *98*, 1358.
(29) Kendall, R. A.; Dunning, T. H.; Harrison, R. J. *J. Chem. Phys.* **1992**, *96*, 6796.
(30) Dunning, T. H. *J. Chem. Phys.* **1989**, *90*, 1007.
(31) Frisch, M. J.; Trucks, G. W.; Schlegel, H. B.; Scuseria, G. E.; Robb, M. A.; Cheeseman, J. R.; Zakrzewski, V. G.; Montgomery, J. A., Jr.; Stratmann, R. E.; Burant, J. C.; Dapprich, S.; Millam, J. M.; Daniels, A. D.; Kudin, K. N.; Strain, M. C.; Farkas, O.; Tomasi, J.; Barone, V.; Cossi, M.; Cammi, R.; Mennucci, B.; Pomelli, C.; Adamo, C.; Clifford, S.; Ochterski, J.; Petersson, G. A.; Ayala, P. Y.; Cui, Q.; Morokuma, K.; Malick, D. K.; Rabuck, A. D.; Raghavachari, K.; Foresman, J. B.; Cioslowski, J.; Ortiz, J. V.; Baboul, A. G.; Stefanov, B. B.; Liu, G.; Liashenko, A.; Piskorz, P.; Komaromi, I.; Gomperts, R.; Martin, R. L.; Fox, D. J.; Keith, T.; Al-Laham, M. A.; Peng, C. Y.; Nanayakkara, A.; Gonzalez, C.; Challacombe, M.; Gill, P. M. W.; Johnson, B.; Chen, W.; Wong, M. W.; Andres, J. L.; Gonzalez, C.; Head-Gordon, M.; Replogle, E. S.; Pople, J. A. *Gaussian 98*, revision A.7; Gaussian Inc.: Pittsburgh, PA, 1998.
(32) Dahoo, P. R.; Berrodier, I.; Raducu, V.; Teffo, J. L.; Chabbi, H.; Lakhlifi, A.; Abouaf-Marguin, L. *Eur. Phys. J. D* **1999**, *5*, 71.
(33) Bentwood, R. M.; Barnes, A. J.; Orville-Thomas, W. J. *J. Mol. Spectrosc.* **1980**, *84*, 391.
(34) Berney, C. V.; Redington, R. L.; Lin, K. C. *J. Chem. Phys.* **1970**, *53*, 1713.
(35) Maçôas, E. M.; Fausto, R.; Pettersson, M.; Khriachtchev, L.; Räsänen, M. *J. Phys. Chem. A* **2000**, *104*, 6956.
(36) Redington, R. L.; Liang, C. K. *J. Mol. Spectrosc.* **1984**, *104*, 25.
(37) Maçôas, E. M.; Fausto, R.; Lundell, J.; Pettersson, M.; Khriachtchev, L.; Räsänen, M. *J. Phys. Chem. A* **2000**, *104*, 11725.